Available online at www.sciencedirect.com
ScienceDirect
Russian Geology and Geophysics 49 (2008) 430–436
RUSSIAN GEOLOGY AND GEOPHYSICS
www.elsevier.com/locate/rgg

A device for shallow frequency-domain electromagnetic induction sounding

A.K. Manstein *, G.L. Panin, S.Yu. Tikunov

Trofimuk Institute of Petroleum Geology and Geophysics, Siberian Branch of the RAS, 3 prosp. Akad. Koptyuga, Novosibirsk, 630090, Russia

Received 2 April 2007; accepted 2 October 2007

Abstract

We have designed a frequency-domain electromagnetic induction sensor for imaging the distribution of electrical conductivity of soils in civil engineering applications. The device implements the ultimate technical feasibility of measuring harmonic signals on the ground surface. Digital recording and narrow bandpass filtering of synchronous detection allows a sufficient measurement accuracy for ~1 μV signals and suppression of power-line noise of more than 100 dB. We suggest practical methods for investigating the characteristics of the sensor and estimating its measurement accuracy.

Keywords: Electrical conductivity of soils; electronic measurement and instrumentation; frequency-domain electromagnetic induction sounding

Introduction

Sounding with alternating electromagnetic fields has been rapidly progressing and broadly used in geophysics for the three recent decades, including frequency-domain electromagnetic induction (FD EMI) sounding. The theory of the method was developed in Russia by L. Vaniyan, A. Kaufman, G. Morozova, L. Tabarovsky, M. Epov, and others (Morozova, 1980).

We have designed a portable electromagnetic sensor (EMS) for frequency-domain electromagnetic induction measurements on the ground surface. It is a 2.5 m long three-coil tool with magnetic dipoles: a transmitter of 0.32 m in diameter on one end and two receivers inside a tube on the other end of the tool. The dipole moments are parallel to one another and perpendicular to the tool long axis. The receivers are opposite connected to provide geometric focusing and are configured in a way to make their moments rather stable at any operating frequency (Manstein et al., 2000).

The sensor (Fig. 1) measures the electrical conductivity of soils to a depth of 10 m below the ground surface for detection of flaws, soil disposal, leakage, pipe lines, cavities, etc. (Balkov et al., 2006). Data acquisition consists in successive conductivity sampling at fourteen discrete frequencies of a harmonic signal (f_i) from 2.5 to 250 kHz; the sounding depth is proportional to $1/f^{0.5}$. See Fig. 2 for an example of EMS data compared to a VES image and Fig. 3 for the instrument block diagram. An acquisition cycle at each frequency includes two steps: first the primary field is measured by an additional coil inside the transmitter and then the sensor records the compensated current response of the ground. The primary field data are used in processing to estimate the transmitter current as a reference for normalizing the real and imaginary components of the secondary field.

Signal extraction principle

The receiver path comprises two antennas $L1$ and $L2$ shielded by electrostatic screens to reduce electric noise (as well as the other electronics), an input amplifier based on an INA163 instrumentation amplifier with a normalized noise coefficient of 1 nV/Hz$^{0.5}$, and a 1–300 kHz bandpass filter (Fig. 3). Such a filter was chosen because the minimum and maximum operation frequencies are, respectively, much higher and lower than the frequencies of power-line noise (50 Hz) and mainly long-wave radio transmission.

We have found the basic design trend for the receiver path in a sensor of this class through the progress of EMS units from one sample to another. Synchronous detection was of best performance due to phase selection and highest sensitivity in measuring two signal components, namely the imaginary component which is in phase with the transmitter current maximum and the real component which is 90° ahead the imaginary component.

* Corresponding author.
E-mail address: MansteinAK@ipgg.nsc.ru (A.K. Manstein)

1068-7971/$ - see front matter © 2008, IGM, Siberian Branch of the RAS. Published by Elsevier B.V. All rights reserved.
doi:10.1016/j.rgg.2007.10.013

Fig. 1. Working EMS instrument.

The best reception in the presence of noise is known to be provided by a matched filter which uses all a priori information on the signal (Klaassen, 1996). The philosophy behind synchronous detection in the EMI sensor is that a synchronous amplifier requires a reference signal that tells about the frequency and phase of the input signal. This reference signal, square-wave in our case, is generated outside the amplifier. The synchronous detector in our sensor consists of an analog switch detector and a digital bandpass filter inside an ADC unit (Fig. 4).

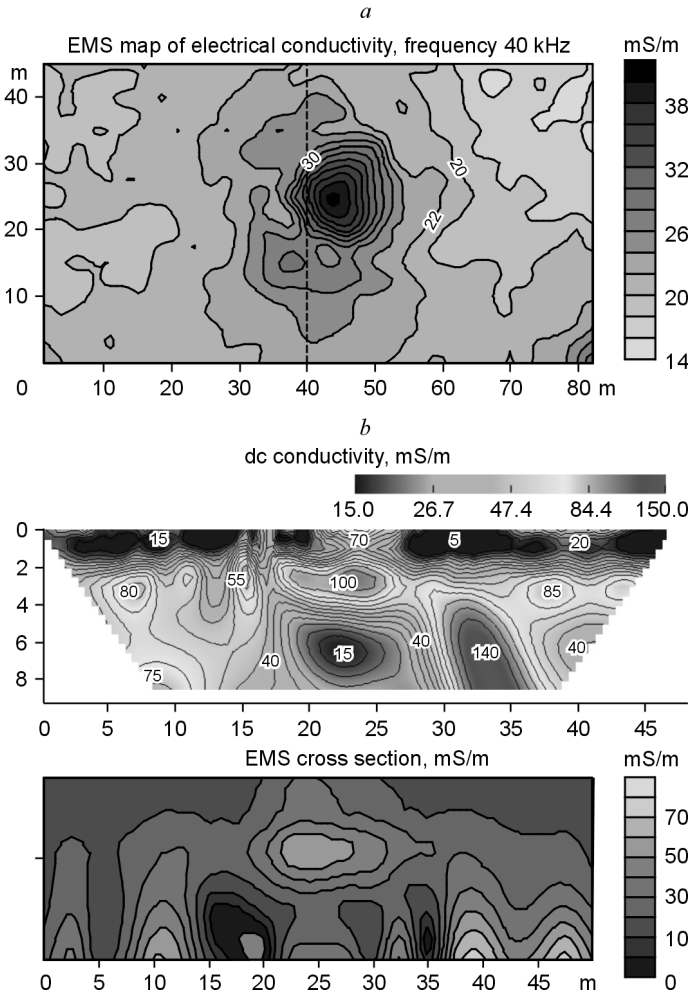

Fig. 2. Map of shallow electrical conductivity. *a* — EMS image, *b* — VES image.

The polarity of the input signal $V_i(t)$ changes at the switch detector output, at a rate controlled by the square reference signal $V_R(t)$. This process can be expressed as the signal

$$V_i(t) = V_i \cos(\omega_i t + \phi)$$

multiplied by the square oscillation taking the values 1 or 0 at the frequency ω_R, which has the mathematical form

$$V_s(t) = \frac{4}{\pi} V_i(t) \left(\cos \omega_R t - \frac{1}{3} \cos 3\omega_R t + \frac{1}{5} \cos 5\omega_R t - \ldots\right).$$

For the noisy periodic input signal $V_i(t)$, at $\omega_i = \omega_R$ (case of synchronous detection), the output signal $V_s(t)$ bears the constant component

$$V_0(t) = \frac{2}{\pi} V_i \cos \phi.$$

Furthermore, the output signal includes harmonic components with their frequencies equal to the sum and the difference of ω_i and all odd-order harmonics of ω_R. The amplitudes of these components have a weight coefficient of $1/n$ for the n-th harmonic of ω_R.

A design feature of the new sensor is that it measures the amplitude of an unmodulated periodic signal in two 90° shifted phases in a narrow band (Balkov and Manstein, 2001). The responses from the receivers or from the primary field sensor are recorded by two simultaneously operated synchronous detectors. The square-wave reference signals are denoted $V_{R1}(t)$ and $V_{R2}(t)$ in Fig. 4. The signals are further transferred to the low-pass filter with a 300 Hz cutoff and the filtered signals proceed to a sigma-delta ADC as a constant component together with remaining noise. We used AD7799, a 3-channel 24-bit sigma delta ADC (AD7799) which has a very low rms noise of 27 nV, an offset error drift vs. temperature of

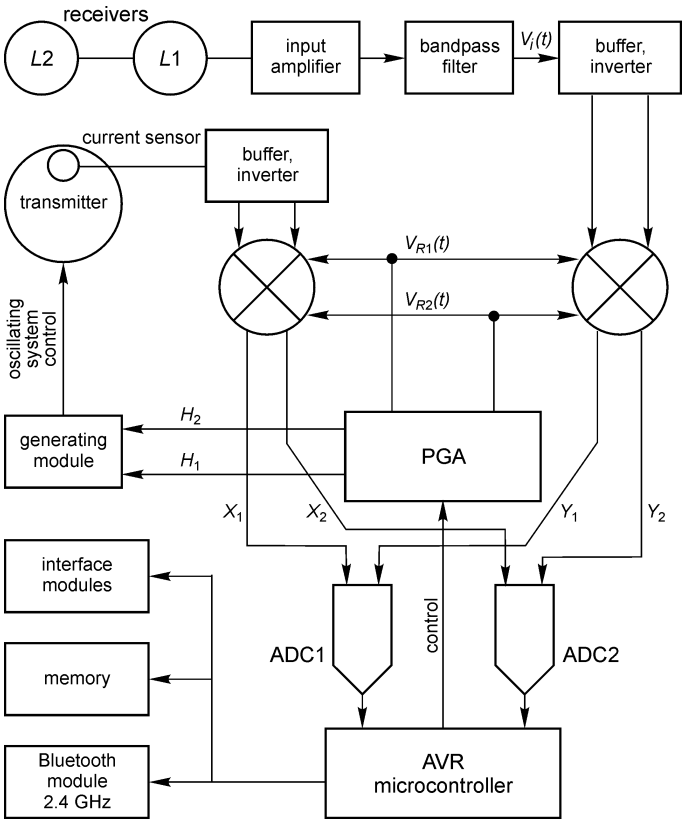

Fig. 3. Block diagram of EMS instrument.

10 nV/°C, and a power supply rejection of no less than 100 dB. At an ADC time of 60 ms, the on-chip digital filter passes from a steady signal to the first minimum (–20 dB) at f_0 = 10 Hz. Thus, the measured components are sensitive to the signal at a bandwidth of $2f_0$ symmetrical relative to the odd-order harmonics of the reference frequency f_R. When detection is performed using signal multiplication and low-pass filtering, the spectrum of the $2f_0$ input signal is transferred to the low-frequency band from 0 to f_0. Synchronous detection allows measuring the amplitude and phase of very low and noisy signals in a relatively narrow bandwidth, that is the case of frequency-domain EMI soundings in which a sinusoidal primary field is generated by a resonant circuit with phase control.

The primary-field signal being much above the noise, the ADC time may be as short as 4 ms, which corresponds to a band of 0–500 Hz (AD7799).

Figure 5 shows a real spectral sensitivity pattern of the switch detector with a $2f_0$ low-pass filter. The spectral sensitivity in our EMS differs in low input harmonics due to the joint effect of the predetection bandpass filter (Fig. 3) and the digital low-pass filter.

The main advantage of the switch detector is that it can be designed to work perfectly over a large range of input frequencies and amplitudes, which is especially useful for noise-flooded signals.

Transmitter control system

The transmitter is a phase-control system. The generation module consists of an excitation unit and a system of coupled excitation and resonant circuits (Fig. 3). The resonant circuit is connected to a switch capacitor unit to achieve resonance at each frequency. The transmitter excites an alternating coherent magnetic field. The source electromagnetic field was recognized empirically to have its phase constant independent of natural soil properties and changing only in the proximity of metal objects.

The generator of reference signals synthesizes excitation signals of the transmitter (H_1, H_2) and paraphase signals of switch detector control ($V_{R1}(t)$, $V_{R2}(t)$). It is implemented on an Atera EPM3064 PGA (Programmable Gate Array) comprising an adjustable ratio divider, a fixed-ratio divider, a control system, and an excitation signal discrimination logic (Fig. 6).

The output signal $V_{R1}(t)$ is a source of signals for ac excitation in the transmitter circuit (see the right panel of Fig. 6 for the output signals).

To assess the accuracy of an EMS device of this kind, one has to estimate the signal repeatability, to measure the receiver path bandwidth, and to investigate the linearity of AD conversion and the dependence of the excitation phase on capacitance change vs. temperature in the transmitter resonant circuit. For this we assumed a temperature change of no more

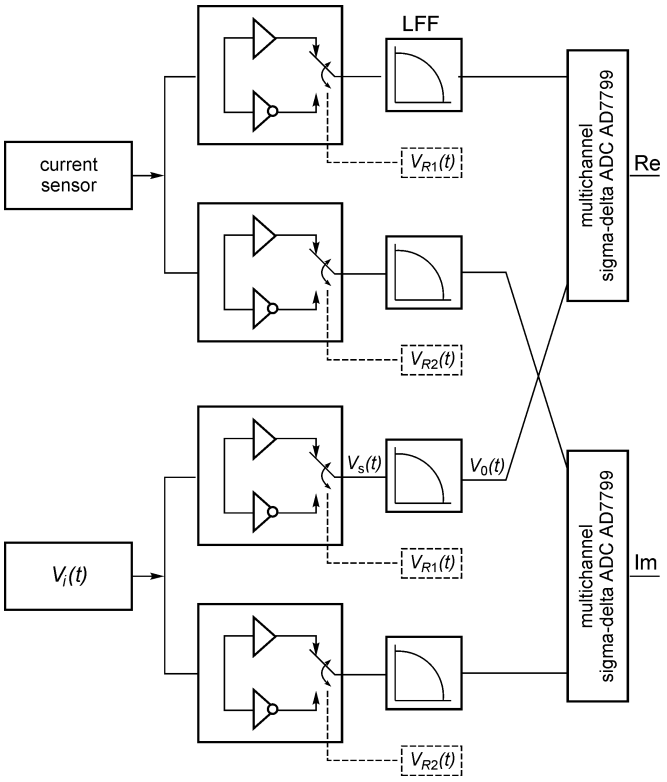

Fig. 4. Block diagram of two-channel synchronous detector.

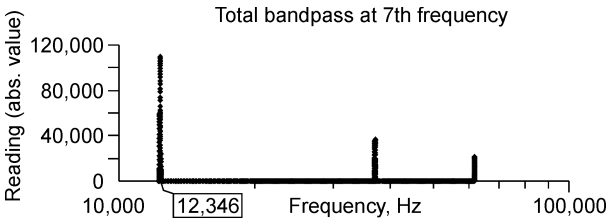

Fig. 5. Experimental spectral sensitivity to input signal.

than ±10 °C and a vanishing temperature-dependent change of the tool's linear dimensions.

Receiver bandpass test

The receiver bandpass was measured during the EMS transmitter off-time. An external source was turned on after power-up and zero reading. The zero reading procedure consists in noise measurement when the on-chip transmitter is off and reception is on both channels (Re and Im). Then the noise (at each operation frequency) was subtracted from the real-time measurements.

A highly stable external source of sinusoidal signals (G3-110) and a multiturn coil generated an alternating magnetic field near the receivers. The instrument was run at one operation frequency and the external source was run at a frequency which was 100 Hz different from the latter. Two signal components were measured and then the external source changed its frequency to make it 98 Hz different from the operation frequency, and so on at every 2 Hz. Thus we measured the predigital receiver frequency response and plotted it as frequency-dependent variations of the recorded signal. The resulting bandpass was 20 Hz ($2f_0$, Fig. 7). In the same way we measured the pass of harmonics. In the case when the external source was on before the sensor turn-on (which corresponds to real operation conditions of permanent noise), the external signal was assumed to be zero.

The receiver bandpass turned out to be the same at all frequencies. See Fig. 7 for a frequency response at 27,779 Hz.

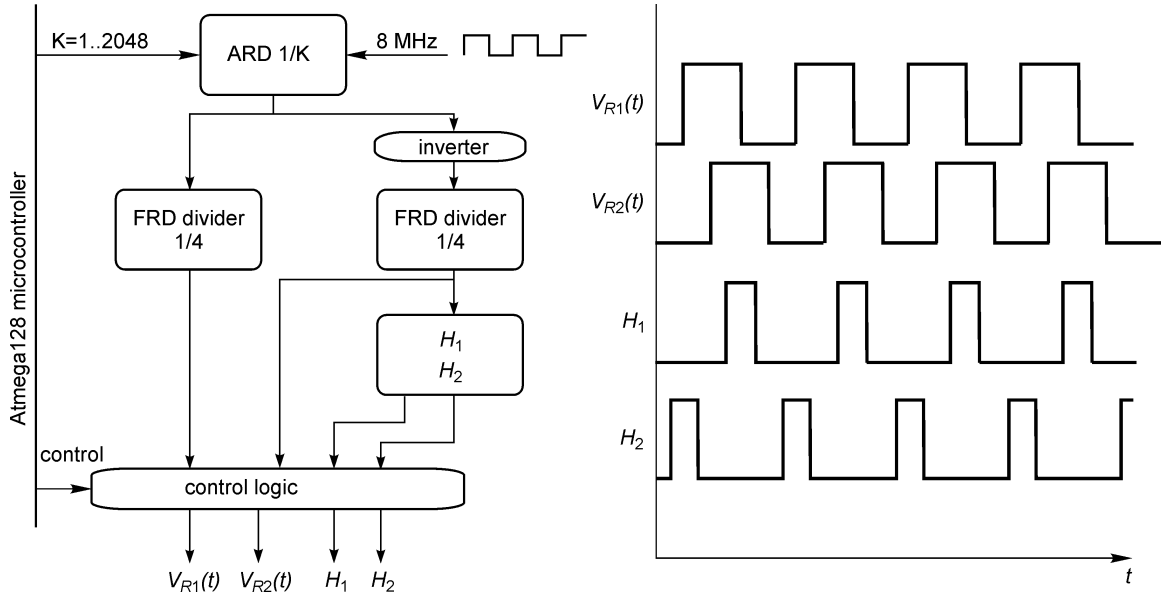

Fig. 6. Control system of EMS transmitter.

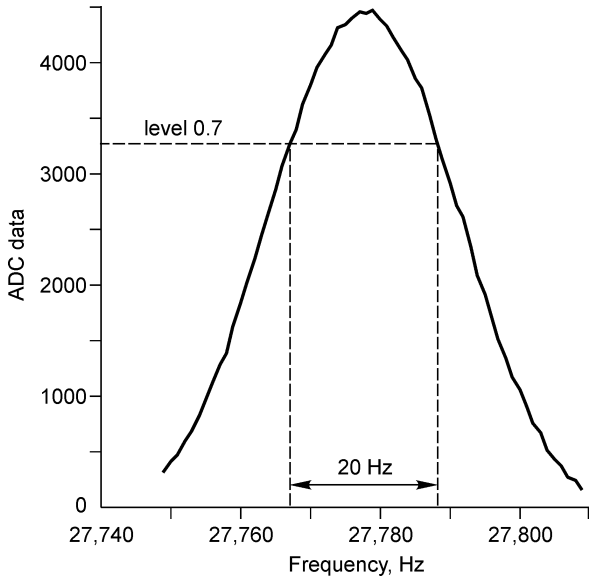

Fig. 7. Bandpass in vicinity of 27,779 Hz.

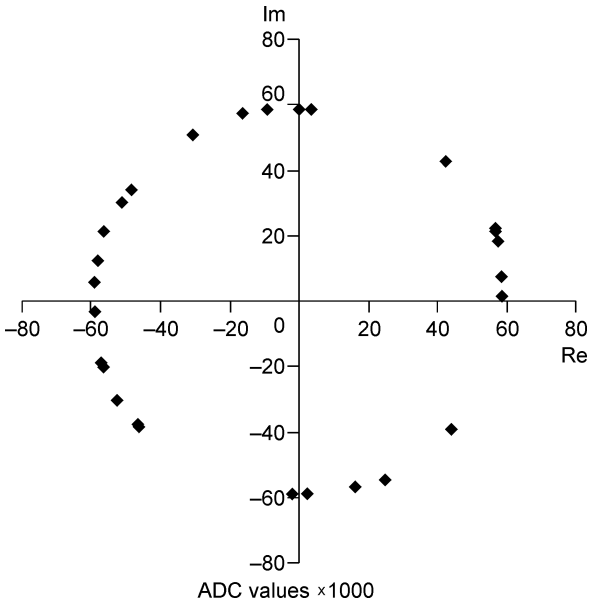

Fig. 8. Randomly measured imaginary and real components of field generated by external source.

ADC linearity

AD conversion of the input signal is linear in the absence of amplitude-phase disturbance in the receiver path. We investigated the linearity of transmission through the receiver circuits (switch detector and ADC) at any phase during the on-chip transmitter off-time. Simultaneously we checked the algorithm of initial signal processing in the microcontroller. The field was excited by an external source, placed near the EMS receivers, with supply from G3-110 sinusoidal current generated at a selected EMS operation frequency. The field was specified at a level not to overload the analog circuits.

It follows from statistical principles that the real and imaginary components of thus measured field look as a circle in the plan view in the absence of disturbance and at randomly chosen measurement start time under continuous external excitation. See the result for one frequency in Fig. 8, which was the same at all other EMS operation frequencies: The points circle about zero (0.0) at a radius deviating for no more than 1.2% from the mean value.

Dependence of excitation phase on capacitance changes vs. temperature in the transmitter resonant circuit

The ambient temperature causes most of disturbance to capacitance. We studied the effect of ±10 °C air temperature change which is enough to account for variations during a working day. For this we measured phase change in a test response relative to that of the transmitter resonant circuit (L) using an air adjustable capacitor (ΔC) joined parallel to the standard EMS capacitor. Measurements were performed on a double-beam electronic oscillograph. See Fig. 9 for the experiment layout. A 6% change of the additional capacitance ΔC relative to C_0 caused a 25° shift of the sinusoidal signal in the display. The time delay was converted to degrees through phase measurements of the wave period in the same display. The test coil had few turns and its frequency response did not disturb the EMS response at all operation frequencies. See the excitation phases (degrees) plotted as a function of the resonance capacitance variations ($\Delta C/C_0$, percent) in Fig. 10. Multiple laboratory measurements of TCC (temperature coefficient of capacitance in the K73-17 capacitor we used) gave a mean of $5 \cdot 10^{-4}$/deg. Taking into account that TCC = $\Delta C/C_0 \Delta T$, where ΔT is the capacitor temperature rise, the ratio $\Delta C/C_0 = 2\%$ corresponds to a temperature rise of 40 °C. Therefore, EMS excitation remains stable at capacitor temperature variations within ±10 °C. An air temperature change of ±20 °C causes ±1° phase change of the excited electromagnetic field, which makes no limitation on the instrument applicability.

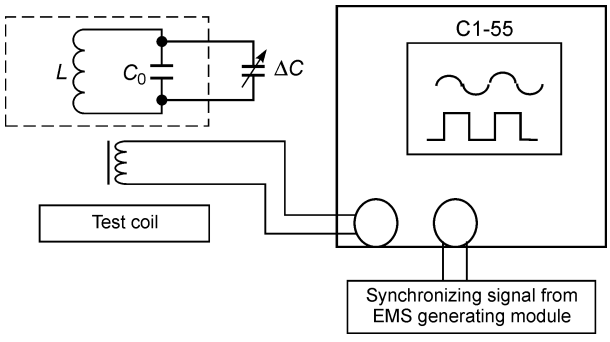

Fig. 9. Measuring excitation phase change as a function of resonant capacitance change. Dashed box frames EMS units.

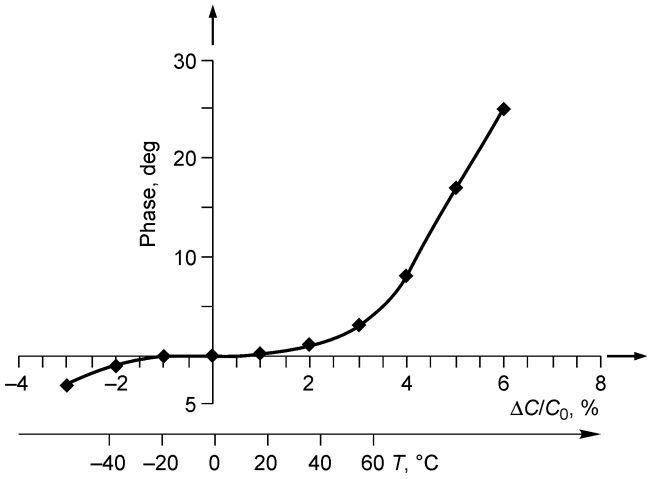

Fig. 10. Excitation phase change as a function of resonant capacitance change and tentative temperature scale.

Accuracy of measurements

The accuracy of EMS measurements was checked in tests set up and interpreted in accordance with Russian State Standard and International Standards 5725-2002. The sensor is designed in a way that it reads zero (zero response) at no input signal, with a repeatability error of no more than three five-digit decimal units. The zero response (often called free-air response), which is a systematic error component in the conditions of repeatability, is measured as a function of frequency by raising the sensor 10 m above the ground. The zero response is stored in the sensor and subtracted from the measurements in real-time during a survey.

The accuracy of EMS measurements being independent of the executing laboratory, statistical analysis is applicable to its testing, according to the State Standard recommendations. In the model for statistical analysis, each measurement (y) is represented by the sum $y = m + e$, where m is the overall mean (mathematical expectation) and e is the repeatability random error component.

The data set used for processing was filtered from spikes.

The random error repeatability limits were estimated experimentally and the results of the tests were plotted as error histograms at several signal strengths (~500; ~3000; >25,000). Data samples consisted of more than 200 Re(U_i) and Im(U_i) values at each of fourteen frequencies. The arithmetic mean (U) was assumed to be the most probable signal value. The histograms were approximated by the normal distribution function

$$\varphi(U_i) = e^{-(U_i - U/\sigma)^2},$$

where U_i is the signal measured at the i-th of 200 realizations and σ is the rms error. The rms error and the mathematical expectation of a random value have the same dimension as the measured parameter. To plot the histograms, we calculated relative deviation from the mean for each U_i and constrained its range between the minimum and maximum $\pm(U_i - U)$; then we specified $\Delta\sigma$ (sampling interval) and divided $\pm(U_i - U)$ by $\Delta\sigma$, which defined the column width along the x axis; then we calculated the number of events (N) in each column as the number of measurements with the given deviation from the mean and found the maximum number of events N_{max}. Thus, the values along the y axis are the relative frequencies of

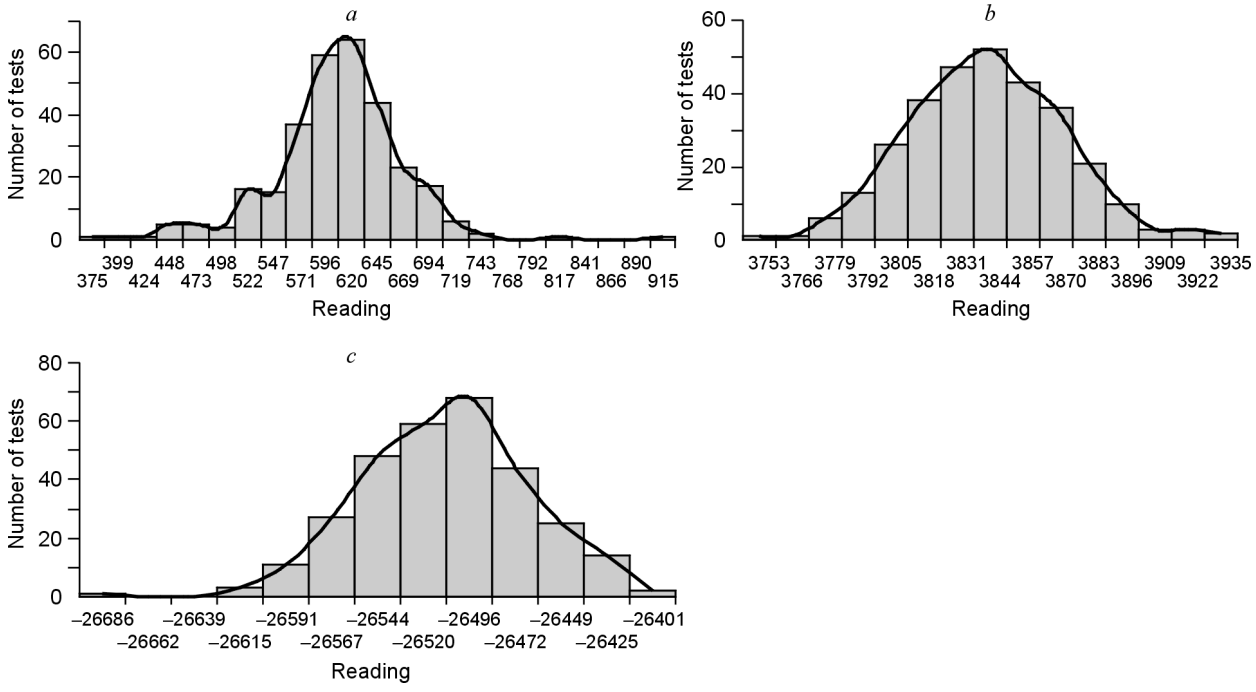

Fig. 11. Error histograms. *a–c* are explained in text.

events N/N_{max} and those along the x axis are percent relative errors $(U_i - U)/U$.

See Fig. 11 for histograms resulting from multiple EMS measurements at different frequencies. The envelope through the centers of columns gave a pattern corresponding to a normal Gaussian distribution (Levin, 1960). The histograms of case EMS measurements at a 95% confidence level show that the rms error is the greatest (10.2% of signal, 60.9 units) for a mean signal of 596.2 (Fig. 11, *a*) and less at signals about 3835 (30.4 units, with an uncertainty of ±0.8%, Fig. 11, *b*) and 26520 (43.2 units, ±0.16%, Fig. 11, *c*).

These estimates are valid for the electromagnetic noise that was present during the tests. Faster calculation of σ is possible by estimating random variance about the mean. When applied in the field, this estimation gives an idea of external noise in addition to the confidence interval of measurements.

Laboratory tests of the receiver sensitivity yielded a mean of 10 nV per five-digit decimal unit. With a maximum corresponding to the highest signal of 65,535, a maximum allowable error of ±5% and a rms error of 5 units, the lowest measurable signal is ±1 μV and the highest signal, with regard to gain, is ±310 μV.

We derived a formula for estimating the measurement accuracy according to the State Standard and applied it to six levels of the test signal:

$$\delta = \pm\left(0.03 + \frac{87.4}{m}\right)\%,$$

where m is the measured signal strength in five-digit decimal ADC units.

Conclusions

Thus, we have demonstrated one possible implementation of a portable electromagnetic sensor (EMS) for frequency-domain electromagnetic induction measurements. The operation experience shows high repeatability of EMS-measured responses at frequencies to 300 kHz. The synchronous detection we use provides linear AD conversion. The suggested method of accuracy assessment is well applicable to instruments of this kind.

The study was supported by grant 06-06-80295a from the Russian Foundation for Basic Research and was carried out as part of SB RAS Interdisciplinary Integration Project 109.

References

AD7799 Preliminary Technical Data. Site of Analog Device Company, www.analog.com.

Balkov, E.V., Manstein, A.K., 2001. A three-coil frequency-domain electromagnetic induction sensor. Geofizicheskii Vestnik EAGO 12, 17–20.

Balkov, E.V., Manstein, A.K., Chemyakina, M.A., Manstein, Yu.A., Epov, M.I., 2006. An experience of using frequency-domain EMI soundings for archaeological geophysical applications. Geofizika 1, 43–50.

Klaassen, K.B., 1996. Electronic Measurement and Instrumentation. Cambridge University Press, New York.

Levin, V.I., 1960. Methods of Mathematical Physics [in Russian]. Uchpedgiz, Moscow.

Manstein, A.K., Epov, M.I., Voevoda, V.V., Sukhorukova, K.V., 2000. A Method of Frequency-Domain EMI Soundings [in Russian]. Patent of the Russian Federation, N 2152058 C1, G 01 V3/10, 24.06.98, Bull. No. 18.

Morozova, G.M. (Ed.), 1980. Dipole Frequency-Domain EM Soundings of a Two-Layer Earth. Methodological Guidelines [in Russian]. Book 1, IGiG SO AN SSSR, Novosibirsk.

Editorial responsibility: M.I. Epov